J. Eng. Technol. Sci., Vol. 50, No. 6, 2018, 737-757

Calculation of Peak Particle Velocity Caused by Blasting Vibration in Step Topography

Xi Yang*, Yunpeng Zhang, Deqing Gan & Xinyu Wei

North China University of Science and Technology, Hebei Mining Key Laboratory of Development and Safety Technology, Tangshan Hebei 063000, China
*E-mail: 1637798965@qq.com

Abstract. High ground vibrations not only adversely affect the integrity of the structures in a mine area but also create inconvenience for the nearby population. In order to protect the Sanyou Mine slope in Tangshan, China from blasting vibration, the peak particle velocity in step topography must be accurately calculated. At present, the reflection coefficient of the stress wave at free interface is not considered in the equation for calculating the peak particle velocity in step topography. Therefore the accuracy of the peak particle velocity calculation is decreased in the side direction when the reflection coefficient changes. In this study, a 3D finite element analysis was employed for modeling of the blasting vibration. A series of field-testing experiments was conducted to measure the peak particle velocity. Then the reflection coefficient of the stress wave was calculated. Based on this, the principle of the peak particle velocity in step topography was explained. In addition, the application range of the equation in step topography was determined and a new equation for peak particle velocity calculation in step topography is proposed based on the numerical simulation analysis and field-testing experiment.

Keywords: *blasting vibration; fitting analysis; peak particle velocity; reflection coefficient; step topography.*

1 Introduction

In recent years, ground vibration has become a popular research topic due to the growing construction close to vibration sources and the attentiveness of people to their living conditions. For example, vibrations caused by the passage of a train near buildings play an important role [1]. In addition, ground vibration in urban areas due to tunnel excavations seriously affects the structures built on the ground [2]. The ground consumes explosive energy that is applied for rock fracturing. The intensity of the vibration plays a critical role in all kinds of adverse effects. High ground vibrations not only adversely affect the integrity of structures in the mining area but also create inconvenience to the nearby population. In some cases they provoke the population, which can lead to the closure of a mine. High intensity vibration also damages the groundwater and harms the ecology of nearby areas. Blast-induced ground vibration has a

Received July 22nd, 2018, Revised October 25th, 2018, Accepted for publication December 7th, 2018.
 ISSN: 2337-5779, DOI: 10.5614/j.eng.technol.sci.2018.50.6.1

detrimental effect on structures such as buildings, dams, roads, railroads, natural slopes, etc. If ground vibration is not controlled or minimized, it may cause deforestation in the future because of changing the groundwater level, creating landslides, soil loss, etc. [3]. Ground vibration may damage the free face and generate back breaks [4]. Back breaks can create problems while drilling the next blast round and generate over-sized boulders [5]. This adversely affects the economics of the mine, hampers production and endangers the economic development of the surrounding area. Hence, it is important to measure and control blasting vibration with great accuracy [6].

The study of blasting vibration propagation in step topography is an important basis for engineering blasting design and peak particle velocity calculation. In this field, the Sadaovsk equation is widely used. Using stress wave theory, Wenbo Lu improved the peak particle velocity attenuation equation [7]. Yunzhang Rao calculated and analyzed the peak particle velocity attenuation law by SPSS software [8]. Tao Lu used a nonlinear fitting method to analyze the parameters of the peak particle velocity attenuation equation [9]. Jianhua Hu studied the law of blasting vibration attenuation under single-hole blasting based on a multiple linear regression method [10]. Many experts and scholars have used genetic algorithms [11-15], artificial neural networks [16-20] and other analytical methods to fit the peak particle velocity attenuation equation with high precision. Based on the dimensional analysis method, Hai Tang and other experts arrived at the peak particle velocity calculation equation for step topography [21]. It is as follows:

$$V = k_1 k_2 \left(\frac{\sqrt[3]{Q}}{R}\right)^{\beta_1} \left(\frac{H}{R}\right)^{\beta_2} \tag{1}$$

where k_1 denotes the field coefficient, k_2 denotes the influence coefficient of the convex geomorphology such as the slope, β_1 denotes the attenuation coefficient, Q denotes the charge of the explosive, R denotes the blasting distance, H denotes the elevation, and V denotes the peak particle velocity.

At present, the equation for calculating the peak particle velocity in step topography is mainly based on Eq. (1). However, the reflection coefficient of the stress wave at the free interface is not considered in this equation. Thus, it is more accurate when using it to calculate the peak particle velocity in the positive direction of the explosion zone, when the reflection coefficient does not change. The accuracy of the peak particle velocity calculation is decreased in the side direction when the reflection coefficient changes. The reflection coefficient of the stress wave at the free interface is calculated according to the propagation law of the stress wave. The principle of the above phenomena was analyzed in this study. The application range of Eq. (1) is proposed in this

paper, as well as a new method for calculating the peak particle velocity in step topography.

2 Reflection of Plane Waves on Free Interface

Create a coordinate system as shown in Figure 1. The free interface is represented by $X_3 = 0$. The elastic properties of the rock mass in the half-space are known and the longitudinal and shear wave velocities are known, which are denoted by α and β. The influence of the atmospheric pressure above the free interface is ignored.

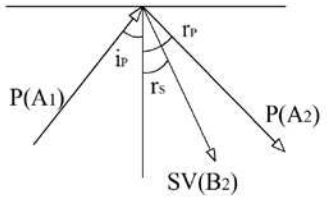

Figure 1 Reflection principle.

Without loss of generality, it is assumed that the incident wave is a simple harmonic plane P wave, which incidents at an angle i_P to the free interface [22,23]:

$$u_{P1} = \nabla\varphi_1, \varphi_1 = A_1 e^{i(x_1 k_{P1} \sin i_P - x_3 k_{P1} \cos i_P) - i\omega_{P1} t} \tag{2}$$

$$\begin{cases} \dfrac{\partial^2 u}{\partial t^2} = (\lambda + \mu)\nabla(\nabla \bullet u) + \mu\nabla^2 u \\ P_{32}\big|_{X_{3=0}} = 0 \end{cases} \tag{3}$$

A_1, W_{P1}, i_P are known as constants. The total displacement field $u(r,t)$ that meets the following equation will be calculated. According to the previous analysis, the potential function can be used to convert the problem of the solution of two scalar functions (φ and ψ_2). Using the semi-inverse method, according to the physical properties of the problem, a number of unknowns can be theorized so that the problem is greatly simplified and then the remaining unknowns can be set by the equation and edge conditions. First, it can be theorized that there is a reflection of the simple harmonic plane wave. At the same time, according to the principle of symmetry, nothing happens to the X_2. So we get the following form solution:

$$u = u_{P1} + u_{P2} + u_{SV2} = \nabla\varphi_1 + \nabla\varphi_2 + \nabla \times \psi_2, \nabla \bullet \psi_2 = 0 \tag{4}$$

$$\varphi_1 = A_1 e^{i(x_1 k_{P1} \sin i_P - x_3 k_{P1} \cos i_P) - i\omega_{P1} t} \tag{5}$$

$$\varphi_2 = A_2 e^{i(x_1 k_{P2} \sin i_P - x_3 k_{P2} \cos i_P) - i\omega_{P2} t} \tag{6}$$

$$\psi_2 = B_2 e^{i(x_1 k_{S2} \sin r_S - x_3 k_{S2} \cos r_S) - i\omega_{S2} t} \tag{7}$$

The subscript 1 corresponds to the incident wave while the subscript 2 corresponds to the reflected wave. If we substitute $u(r,t)$ into the wave equation validation, we get the solution of the wave equation. The form solution, which is structured by d'Alembert's solution, naturally satisfies the wave equation. Substituting the edge conditions $x_3 = 0$ into the wave equation validation, the following results are obtained:

$$\begin{cases} -2\dfrac{\sin i_P}{\alpha}\dfrac{\cos i_P}{\alpha}\varphi_1 + 2\dfrac{\sin r_P}{\alpha}\dfrac{\cos r_P}{\alpha}\varphi_2 + (\dfrac{\sin r_S}{\beta})^2\psi_2 - (\dfrac{\cos r_S}{\beta})^2\psi_2 = 0 \\ (\dfrac{\alpha^2-\beta^2}{2\beta^2})\dfrac{1}{\alpha^2}(\varphi_1+\varphi_2) + (\dfrac{\cos i_P}{\beta})^2\varphi_1 + (\dfrac{\cos r_P}{\alpha})^2\varphi_2 + \dfrac{\sin r_S}{\beta}\dfrac{\cos r_S}{\beta}\psi_2 = 0 \\ Oe^{ix_1 k_{P1}\sin i_P - i\omega_{P1}t} = Pe^{ix_1 k_{P2}\sin r_P - i\omega_{P2}t} + Qe^{ix_1 k_{S2}\sin r_S - i\omega_{S2}t} \end{cases} \tag{8}$$

O, P, Q are all functions that contain A_1, A_2, B_2, k_{P1}, k_{P2}, k_{S2}, ω_{P1}, ω_{P2}, ω_{S2}, λ and μ, which are all constants. Only x_1 and t are variables. Because the edge conditions for any x_1 and t are established, we have:

$$\omega_{P1} = \omega_{P2} = \omega_{S2} \tag{9}$$

$$\frac{\sin i_P}{\alpha} = \frac{\sin r_P}{\alpha} = \frac{\sin r_S}{\beta} \tag{10}$$

$i_P = r_P$, $\omega_{P1} = \omega_{P2} = \omega_{S2}$, $r_S = \arcsin(\beta \sin i_P/\alpha)$ are known, the form solution is further simplified as:

$$\varphi_1 = A_1 e^{i(x_1 k_{P1} \sin i_P - x_3 k_{P1} \cos i_P) - i\omega_{P1} t} \tag{11}$$

$$\varphi_2 = A_2 e^{i(x_1 k_{P1} \sin i_P - x_3 k_{P1} \cos r_P) - i\omega_{P1} t} \tag{12}$$

$$\psi_2 = B_2 e^{i(x_1 k_{S1} \sin r_S - x_3 k_{S1} \cos r_S) - i\omega_{P1} t} \tag{13}$$

Only A_2 and B_2 are unknown. The relationship between A_2, B_2 and A_1 can be solved by substituting the form solution into the edge conditions again. The reflection coefficient can be calculated as follows:

$$\begin{cases} F_{PP} = \dfrac{A_2}{A_1} = \dfrac{\beta^2 \sin 2i_P \sin 2r_S - \alpha^2 \cos^2 2r_S}{\beta^2 \sin 2i_P \sin 2r_S + \alpha^2 \cos^2 2r_S} \\ F_{PS} = \dfrac{B_2}{A_1} = \dfrac{-2\beta^2 \sin 2i_P \cos 2r_S}{\beta^2 \sin 2i_P \sin 2r_S + \alpha^2 \cos^2 2r_S} \end{cases} \tag{14}$$

According to the relationship between the displacement and the displacement function, the displacement reflection coefficient can also be given:

$$\begin{cases} f_{PP} = \dfrac{|\nabla \phi_2|}{|\nabla \phi_1|} = F_{PP} \\ f_{PS} = \dfrac{|\nabla \psi_2|}{|\nabla \phi_1|} = \dfrac{\alpha}{\beta} F_{PS} \end{cases} \tag{15}$$

$$\begin{cases} f_{PP} = \dfrac{\beta^2 \sin 2i_P \sin 2r_S - \alpha^2 \cos^2 2r_S}{\beta^2 \sin 2i_P \sin 2r_S + \alpha^2 \cos^2 2r_S} \\ f_{PS} = \dfrac{-2\alpha\beta \sin 2i_P \cos 2r_S}{\beta^2 \sin 2i_P \sin 2r_S + \alpha^2 \cos^2 2r_S} \end{cases} \tag{16}$$

With the same mathematical method it is possible to solve the problem of the plane SV wave and the plane SH wave travel to the free surface. In particular when the plane SH wave incidents to the free surface, whose displacement reflection coefficient always satisfies $f_{HH'}$=1. Similarly, the reflection coefficient of the SV wave to the free surface is as follows:

$$\begin{cases} f_{SS} = \dfrac{\beta^2 \sin 2i_P \sin 2r_S - \alpha^2 \cos^2 2r_S}{\beta^2 \sin 2i_P \sin 2r_S + \alpha^2 \cos^2 2r_S} \\ f_{SP} = \dfrac{2\alpha\beta \sin 2r_S \cos 2r_S}{\beta^2 \sin 2i_P \sin 2r_S + \alpha^2 \cos^2 2r_S} \end{cases} \tag{17}$$

3 Numerical Simulation Analysis

3.1 Model Establishment

Based on the actual slope of the Sanyou Mine in Tangshan, China, the calculation model is structured as shown in Figure 2. The model contains three steps and each with 24 m height, a slope angle of 70°, a step platform width of 6 m, while the model width is 50 m and the simulation time is 600 μs. The dividing grid is as shown in Figure 2.

Figure 2 Calculation model.

The propagation velocity of the blasting stress wave can be affected by the initial stress, but the propagation direction cannot be affected by the initial stress. In this paper, the peak particle velocity under different incidence angles is discussed. The incidence angle is mainly affected by the propagation direction, so there is no need to consider the initial stress. In the geological survey no large-scale stratification was found in the study area and the rock slope integrity is better than others. Hence it was assumed that the model material is a continuous, homogeneous, non-initial stress and isotropic elasto-plastic material in the simulation process. The specific mechanical parameters of the material are shown in Table 1. The corresponding longitudinal wave velocity and shear wave velocity are 4297 m/s and 2281 m/s. The remaining surfaces of the model are non-reflective boundaries except for the step surfaces.

Table 1 Mechanical parameters of rock.

Material	Volume (cm^3)	Quality (g)	Density ($g \cdot cm^{-3}$)	Modulus of elasticity (GPa)	Poisson ratio	Yield strength (GPa)
Rock	397.70	1021.02	2.6	40	0.25	0.1

3.2 Analysis of Data

3.2.1 Calculation of Reflection Coefficient

The whole slope surface is a reflecting surface. The reflection coefficient of the P wave at the free interface can be calculated by Eq. (16). The relationship between the incident angle and the reflection coefficient of the P-wave reflecting P-wave is shown in the Figure 3. The relationship between the incident angle and the reflection coefficient of the P-wave reflecting SV-wave is shown in Figure 4. Figure 5 is a superposition of Figure 3 and Figure 4. The negative sign indicates the direction.

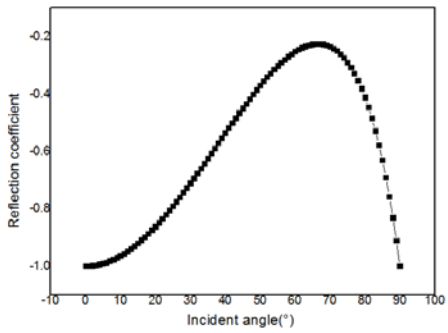

Figure 3 Reflection coefficient of the incident P-wave and the reflecting P-wave.

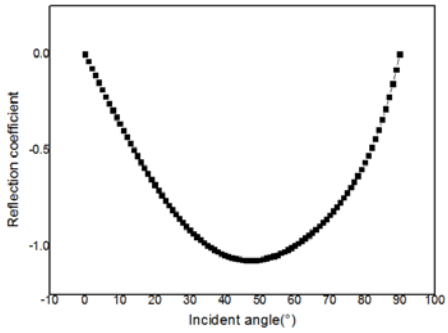

Figure 4 Reflection coefficient of the incident P-wave and the reflecting SV-wave.

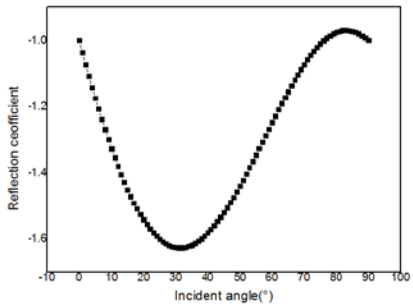

Figure 5 Reflection coefficient of the P-wave.

The reflection coefficient of the SV wave at the free interface can be calculated by Eq. (17). The relationship between the incident angle and the reflection coefficient of the SV-wave reflecting SV-wave is shown in the Figure 6. The relationship between the incident angle and the reflection coefficient of the SV-

wave reflecting P-wave is shown in Figure 7. Figure 8 is a superposition of Figures 6 and 7. The negative sign indicates the direction.

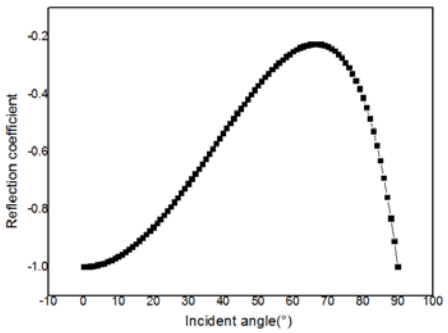

Figure 6 Reflection coefficient of the incident SV-wave and the reflecting SV-wave.

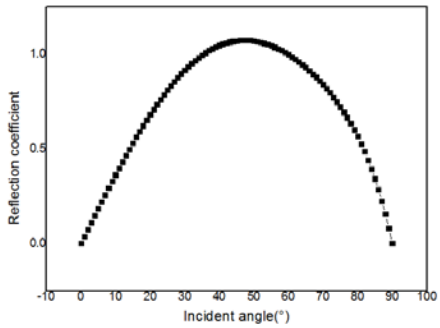

Figure 7 Reflection coefficient of the incident SV-wave and the reflecting P-wave.

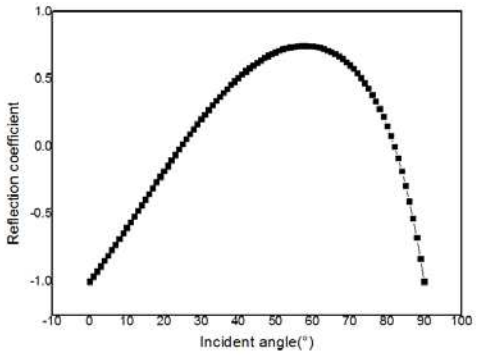

Figure 8 Reflection coefficient of the SV-wave.

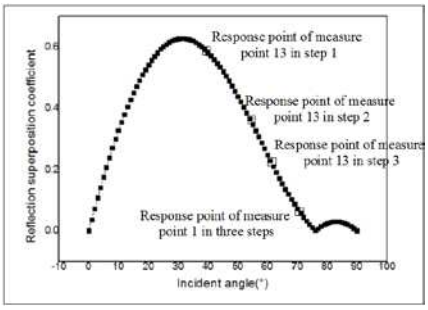

Figure 9 Reflection superposition coefficient of the P-wave.

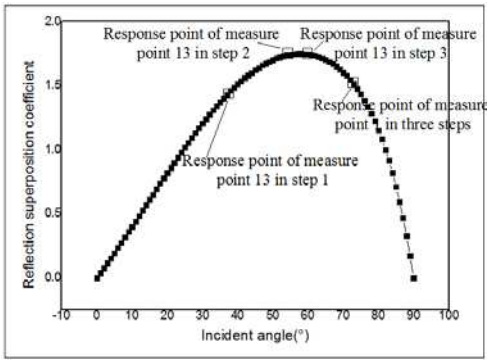

Figure 10 Reflection superposition coefficient of the SV-wave.

Figure 9 shows the reflection superposition coefficient of the P-wave and Figure 10 shows the reflection superposition coefficient of the SV-wave. According to the measuring point arrangement in Figure 14, the velocity diagram of each step is shown as Figure 11. The response points of the measure points in Figure 14 are shown in Figures 9 and 10.

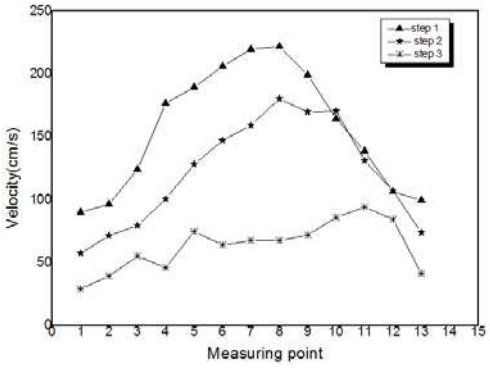

Figure 11 Velocity diagram.

When the stress wave propagates at the free interface there will be reflections on the free surface. Moreover, the reflection coefficient is directly related to the peak particle velocity.

Figures 5 and 8 show that the reflection coefficient first increases and then decreases with the incident angle decreasing within a certain range (the negative sign of the reflection coefficient indicates the direction). The incident angle of the stress waves of the measuring points of each step in Figure 11 is shown in Table 2.

Table 2 Incident angle.

Measure point	Incidence degree of step 1 (°)	Incidence degree of step 2 (°)	Incidence degree of step 3 (°)
1	70	70	70
2	69.33	69.82	69.91
3	67.49	69.33	69.69
4	64.85	68.54	69.33
5	61.74	67.49	68.83
6	58.46	66.25	68.21
7	55.17	64.85	67.49
8	51.98	63.33	66.68
9	48.96	61.74	65.80
10	46.14	60.11	64.85
11	43.52	58.46	63.85
12	41.10	56.81	62.81
13	38.87	55.17	61.74

The reflection coefficients corresponding to the angles in Table 2 gradually increase or increase first and then decrease. As a result, the PPV of the measuring points in Figure 11 gradually increases or increases first and then decreases. However, increasing the distance results in a decrease in the PPV. When the increase of the PPV caused by the change reflection coefficient is larger than the decrease of the PPV caused by the increase of the distance, the phenomenon of the PPV increasing as shown in Figure 11 will appear. In the opposite case, the phenomenon that the PPV decreases in Figure 11 will appear.

3.2.2 Calculation of Peak Particle Velocity

1. Fitting calculation of peak particle velocity in step topography

The measuring points are shown in Figure 12. The test point number follows 1-18 from bottom to top. The corresponding blasting data for each measuring point are shown in Table 3. The blasting data of the numerical simulation were fitted with Eq. (18). The fitting scatter plot of Eq. (18) is shown in Figure 13.

Table 3 Records of blasting data.

Measure point	Charge (kg)	Height (m)	Distance (m)	Actual PPV (cm/s)	Calculated PPV (cm/s)	error
1	4320	4	7.45	338.29	260.18	23.09%
2	4320	8	8.90	130.81	164.55	25.79%
3	4320	12	10.35	111.14	123.96	11.54%
4	4320	16	11.80	92.54	100.61	8.72%
5	4320	20	13.25	79.87	85.18	6.64%
6	4320	24	14.70	84.71	74.12	12.50%
7	4320	28	22.15	52.96	59.36	12.09%
8	4320	32	23.60	42.67	53.84	26.17%
9	4320	36	25.05	44.68	49.33	10.41%
10	4320	40	26.50	57.69	45.58	21.00%
11	4320	44	27.95	60.86	42.40	30.34%
12	4320	48	29.40	57.51	39.66	31.03%
13	4320	52	36.85	33.82	35.19	4.07%
14	4320	56	38.30	28.95	33.30	15.03%
15	4320	60	39.75	25.05	31.62	26.21%
16	4320	64	41.20	27.26	30.11	10.44%
17	4320	68	42.65	29.29	28.75	1.86%
18	4320	72	44.10	29.19	27.51	5.75%

Figure 12 Measuring point arrangement.

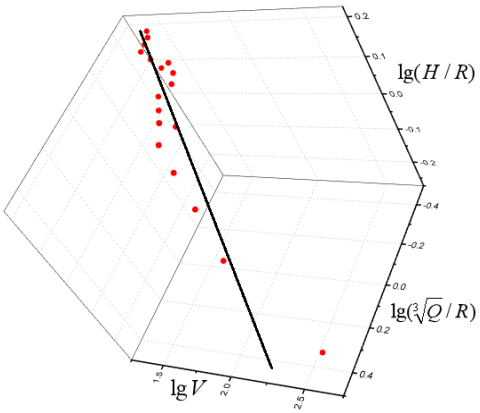

Figure 13 Data fitting results of Eq.(18).

$$V = 89.7(\frac{\sqrt[3]{Q}}{R})^{0.9021}(\frac{H}{R})^{-0.5778}(r^2 = 0.9164) \quad (18)$$

The average error of the calculated result is 15.70%. The error is calculated by:

$$error = \frac{|\text{ActualPPV} - \text{CalculatedPPV}|}{\text{ActualPPV}}$$

The average error is calculated by:

$$\text{average error} = \frac{(error_1 + error_2 + ... + error_n)}{n}$$

The measuring points are shown in Figure 14. The measuring point number follow 1-13 from right to left. The blasting data at the measuring points are shown in Table 4.

Figure 14 Measuring point arrangement.

Table 4 Records of blasting data.

Measure point	Actual PPV of step 1 (cm/s)	Distance (m)	Actual PPV of step 2 (cm/s)	Distance (m)	Actual PPV of step 3 (cm/s)	Distance (m)
1	90.11	14.74	57.51	29.48	29.19	44.22
2	96.40	15.27	71.39	29.75	39.30	44.40
3	123.99	16.77	79.43	30.55	55.34	44.94
4	176.49	19.01	100.53	31.83	46.08	45.82
5	189.36	21.75	128.10	33.54	74.81	47.03
6	206.01	24.84	147.04	35.62	63.97	48.53
7	219.49	28.17	159.08	38.01	67.43	50.31
8	221.52	31.64	180.33	40.66	67.44	52.34
9	199.11	35.23	169.64	43.51	71.82	54.58
10	164.44	38.90	170.27	46.53	85.83	57.02
11	138.54	42.63	131.00	49.69	94.10	59.63
12	106.35	46.40	107.21	52.96	84.35	62.38
13	99.42	50.21	73.75	56.33	41.49	65.26

The above data were fitted and analyzed, and the equation for calculating the peak particle velocity is shown in Eq. (19). The fitting scatter plot of Eq. (19) is shown in Figure 15.

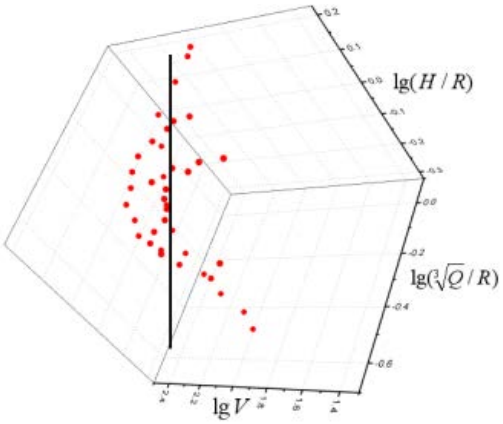

Figure 15 Data fitting results of Eq. (19).

$$V = 201.65(\frac{\sqrt[3]{Q}}{R})^{0.6731}(\frac{H}{R})^{-0.9207}(r^2 = 0.4938) \tag{19}$$

The calculation result of the Eq. (19) and the error are shown in Table 5. The average error of the calculated result was 32.12%. Comparing Eq. (18) with the Eq. (19), the fitting accuracy is high in the positive direction of the explosion area. However, it is greatly reduced in the side direction.

Table 5 Records of blasting data.

Measure point	Calculated PPV of step 1 (cm/s)	error	Calculated PPV of step 2 (cm/s)	error	Calculated PPV of step 3 (cm/s)	error
1	137.67	52.79%	86.34	50.13%	65.72	125.17%
2	138.89	44.07%	86.54	21.21%	65.79	67.40%
3	142.14	14.64%	87.10	9.66%	65.98	19.22%
4	146.61	16.93%	88.00	12.47%	66.30	43.88%
5	151.60	19.94%	89.14	30.41%	66.73	10.81%
6	156.67	23.95%	90.48	38.46%	67.25	5.13%
7	161.61	26.37%	91.95	42.20%	67.85	0.62%
8	166.34	24.91%	93.49	48.15%	68.52	1.61%
9	170.82	14.21%	95.08	43.95%	69.24	3.60%
10	175.06	6.46%	96.67	43.23%	69.99	18.45%
11	179.08	29.26%	98.26	25.00%	70.77	24.79%
12	182.88	71.96%	99.82	6.89%	71.56	15.16%
13	186.48	87.58%	101.35	37.43%	72.37	74.44%

The average error increased from 15.70% to 32.12%. This is because during the process of the stress waves propagating to the side direction of the step, the incident angle constantly changes, which causes changes of the stress wave reflection coefficient. Therefore, Eq. (1) is more accurate in the positive direction of the explosion zone.

2. Gaussian fitting calculation

The Gaussian function ($G_i(x)=A_i\exp[(x-B_i)^2/C_i^2)]$) is applied to fit the data. There are many similarities between Gaussian fitting and polynomial fitting, but there are also some significant differences. Polynomial fitting uses a power function system, while Gaussian fitting uses a Gaussian function system. The Gaussian method makes the calculation of the integral process easy and quick, which is its biggest advantage. We can get the fitting Gaussian function related to the measured data [24-29]. The data in Table 3 were fitted by the Gaussian function and the results are shown as Table 6.

Table 6 Records of blasting data.

Measure point	Calculated PPV of step 1 (cm/s)	error	Calculated PPV of step 2 (cm/s)	error	Calculated PPV of step 3 (cm/s)	error
1	67.31	25.30%	36.02	37.37%	24.98	14.40%
2	89.39	7.27%	47.83	33.00%	33.18	15.58%
3	113.65	8.33%	60.81	23.44%	42.18	23.78%
4	138.35	21.61%	74.03	26.36%	51.35	11.44%
5	161.25	14.84%	86.28	32.65%	59.85	20.00%
6	179.94	12.65%	96.28	34.52%	66.78	4.40%
7	192.24	12.42%	102.86	35.34%	71.35	5.81%
8	196.64	11.23%	105.22	41.65%	72.98	8.23%
9	192.57	3.28%	103.04	39.26%	71.48	0.48%
10	180.57	9.81%	96.62	43.26%	67.02	21.91%
11	162.10	17.00%	86.73	33.79%	60.16	36.06%
12	139.32	31.00%	74.55	30.46%	51.71	38.69%
13	114.65	15.32%	61.35	16.82%	42.55	2.57%

The above data were fitted and analyzed, and the equation for calculating the peak particle velocity is shown in Eq. (20).

$$V = 89.7\left(\frac{\sqrt[3]{Q}}{R}\right)^{0.9021}\left(\frac{H}{R}\right)^{-0.5778} * 74.12e^{-\left[(r-28.08)/27.12\right]^2} \quad (r^2 = 0.6714) \tag{20}$$

The fitting scatter plot of Eq. (20) is shown in Figure 16.

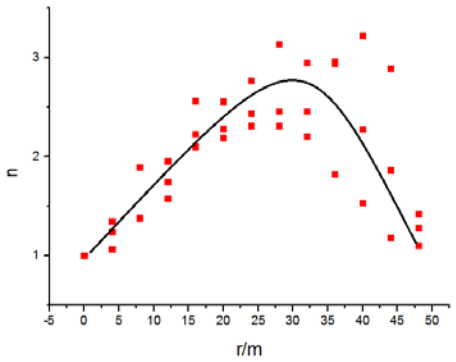

Figure 16 Data fitting results of Eq. (20).

The average error of Gaussian fitting was 21.06%.

$n = V / [89.7(\frac{\sqrt[3]{Q}}{R})^{0.9021}(\frac{H}{R})^{-0.5778}]$, r is the horizontal distance between point 1 and the other measured points. Comparing Eq. (19) with Eq. (20), the accuracy of the calculated result with Eq. (19) was low and the average error was 32.12% while the accuracy of the calculated result with Eq. (20) is high and the average error was 21.06%.

4 Experiment Analysis

As shown in Figure 17, three steps in the open pit were selected. There were five measuring points. The height of each of the steps was 24 m, the step width was about 8 m, and the slope angle was about 70°. The blasting data records for each measuring point are shown in Table 7.

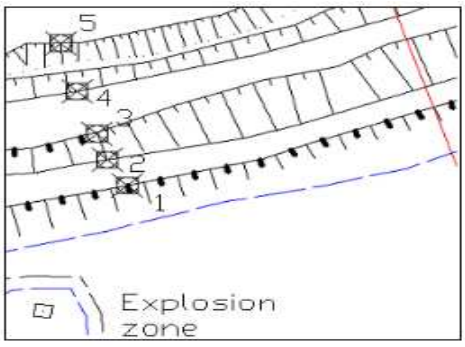

Figure 17 Measuring point arrangement.

Table 7 Records of blasting data.

Measure point	Charge (kg)	Height (m)	Distance (m)	Actual PPV (cm/s)	Calculated PPV (cm/s)	error
1	200	24	37	8	8.06	0.81%
2	200	24	48	5.47	4.96	9.40%
3	200	48	58	4.63	3.60	22.35%
4	200	48	66	4.1	2.82	31.14%
5	200	72	84	1.76	1.83	4.15%
1	180	24	37	5.95	7.56	27.14%
2	180	24	48	3.66	4.65	27.01%
3	180	48	58	3.27	3.37	3.12%
4	180	48	78	1.88	1.94	3.05%
5	180	72	84	1.35	1.72	27.36%
1	150	24	79	2.07	1.64	20.85%
2	150	24	95	0.96	1.16	20.87%
3	150	48	105	1.14	0.99	12.77%
4	150	48	117	0.67	0.81	21.23%
5	150	72	129	0.83	0.69	16.89%
1	160	24	74	2.27	1.93	15.17%
2	160	24	85	1.52	1.49	2.25%
3	160	48	94	1.33	1.27	4.35%
4	160	48	108	0.83	0.98	18.21%
5	160	72	120	0.72	0.82	14.07%

The data were fitted and analyzed, and the equation for calculating the peak particle velocity is Eq. (21). The fitting scatter plot of Eq. (21) is shown in Figure 18.

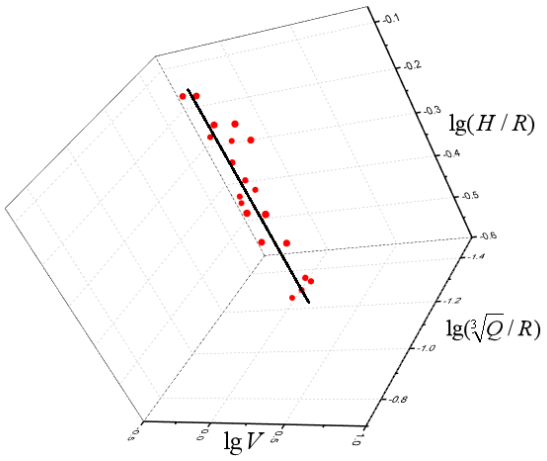

Figure 18 Data fitting results of Eq. (21).

$$V = 237.79(\frac{\sqrt[3]{Q}}{R})^{1.8231}(\frac{H}{R})^{0.0476}(r^2 = 0.9416) \quad (21)$$

The average error of the calculated peak particle velocity was 15.11%. As shown in Figure 19, there were six measuring points on the step. The distance between two points was 35 m. Point 1 was in the positive direction of explosion area. The height of the step was 24 m and its width was about 8 m, while the slope angle was about 70°. The blasting data records for each measuring point are shown in Table 8. The data were fitted and analyzed, and the equation for calculating the peak particle velocity is Eq. (22). The fitting scatter plot of Eq. (22) is shown in Figure 20.

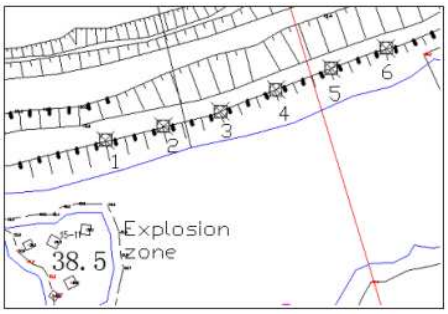

Figure 19 Measuring point arrangement.

Table 8 Records of blasting data.

Measure point	Charge (kg)	Height (m)	Distance (m)	Actual PPV (cm/s)	Calculated PPV (cm/s)	error
1	200	24	37	8	8.06	0.81%
2	200	24	48	5.47	4.96	9.40%
3	200	48	58	4.63	3.60	22.35%
4	200	48	66	4.1	2.82	31.14%
5	200	72	84	1.76	1.83	4.15%
1	180	24	37	5.95	7.56	27.14%
2	180	24	48	3.66	4.65	27.01%
3	180	48	58	3.27	3.37	3.12%
4	180	48	78	1.88	1.94	3.05%
5	180	72	84	1.35	1.72	27.36%
1	150	24	79	2.07	1.64	20.85%
2	150	24	95	0.96	1.16	20.87%
3	150	48	105	1.14	0.99	12.77%
4	150	48	117	0.67	0.81	21.23%
5	150	72	129	0.83	0.69	16.89%
1	160	24	74	2.27	1.93	15.17%
2	160	24	85	1.52	1.49	2.25%
3	160	48	94	1.33	1.27	4.35%
4	160	48	108	0.83	0.98	18.21%
5	160	72	120	0.72	0.82	14.07%

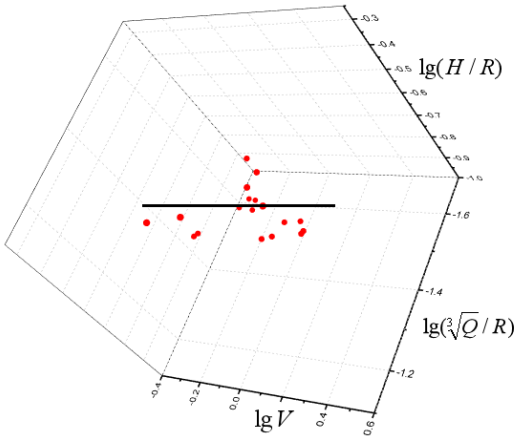

Figure 20 Data fitting results of Eq. (22).

$$V = 6.01(\frac{\sqrt[3]{Q}}{R})^{0.2006}(\frac{H}{R})^{0.6539}(r^2 = 0.5091) \tag{22}$$

The average error of the calculated peak particle velocity was 34.3%. Comparing Eq. (21) with Eq. (22), the fitting accuracy was of Eq. (21) was high in the positive direction of the explosion area. However, the accuracy of the fitting was significantly reduced and the average error increased from 15.11% to 34.3% in the side direction. The above data were fitted and analyzed by the Gaussian function, and the equation for calculating the peak particle velocity was Eq. (23). The fitting scatter plot of Eq. (23) is shown in Figure 21.

$n = V / [237.79(\frac{\sqrt[3]{Q}}{R})^{1.8231}(\frac{H}{R})^{0.0476}]$, r is the horizontal distance between point 1 and the other measured points.

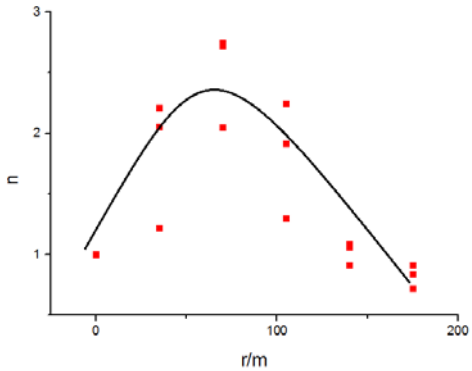

Figure 21 Data fitting results of Eq. (23).

$$V = 237.79(\frac{\sqrt[3]{Q}}{R})^{1.8231}(\frac{H}{R})^{0.0476} * 2.294e^{-[(r-72.67)/83.02]^2} \ (r^2 = 0.7445) \qquad (23)$$

The average error of the calculated peak particle velocity was 24.43%. Comparing Eq.(22) with Eq.(23), the average error of Eq.(22) was high, and the average error was 34.3%. However, the average error of Eq.(23) was low and the average error was 24.43%. The experimental results were the same as the simulation results, and the accuracy of the analysis was verified. The peak particle velocity is affected by many factors. This still requires further research. Although there were still some large errors (larger than 20%), the accuracy of calculating the peak particle velocity with the new method is greatly improved.

5 Conclusion

In this study, a 3D finite element analysis and a series of field-testing experiments was done to determine the effect of the reflection coefficient on the peak particle velocity. Based on the calculation of the reflection coefficient of the plane wave at the free interface, the variation law of the reflection coefficient under the changing incident angle was obtained. Based on this, the principle of the changing peak particle velocity in step topography was explained. There are different trends in the peak particle velocity because of the varying reflection coefficient. At present, the reflection coefficient of the stress wave at the free interface is not considered by the equation for calculating the peak particle velocity in step topography. Therefore it is more accurate when using it to calculate the peak particle velocity in the positive direction of the explosion zone when the reflection coefficient does not change, but the accuracy of the peak particle velocity calculation decreases in the side direction when the reflection coefficient changes. Therefore, under the premise of considering the varying reflection coefficient, a new equation for calculating the peak particle velocity in step topography was proposed based on the numerical simulation analysis and field-testing experiments. It can be used to get an accurate peak particle velocity in different directions in step topography, so the slopes of the Sanyou Mine in Tangshan, China and the surrounding structures can be better protected in the future. It also can be applied to other mines in a similar situation.

Acknowledgements

The research was mainly supported by the National Natural Science Foundation of China (51374087) and the Natural Science Foundation of Hebei Province (E2016209388). The authors would also like to acknowledge the anonymous reviewers who played a significant role in shaping and improving the manuscript.

References

[1] Hesami, S., Ahmadi, S. & Ghalesari, A.T., *Numerical Modeling of Train-Induced Vibration of Nearby Multi-story Building: A Case Study*, Journal of Civil Engineering, **20**(5), pp. 1701-1713, 2016.

[2] Hesami, S., Ahmadi, S., Ghalesari, A.T. & Hasanzadeh, A., *Ground Surface Settlement Prediction in Urban Areas due to Tunnel Excavation by the NATM*, Electr. J. Geotech. Eng, **18**, pp. 1961-1972, 2013.

[3] Khandelwal, M. & Singh, T.N., *Prediction of Blast-induced Ground Vibration Using Artificial Neural Network*, Int. J. Rock Mech. Min. Sci., **46**, pp. 1214-1222, 2009.

[4] Duvall, W.I., Johnson, C.F. & Meyer A.V.C., *Vibrations from Blasting at Iowa Limestone Quarries*, USBM Rep Invest, **28**, pp. 6270, 1963.

[5] Monjezi, M. & Dehghani, H., *Evaluation of Effect of Blasting Pattern Parameters on Back Break using Neural Networks*, Int J Rock Mech Min Sci, **45**, pp. 1446-1453, 2008.

[6] Dehghani, H. & Ataee-pour, M., *Development of a Model to Predict Peak Particle Velocity in a Blasting Operation*, Int J Rock Mech Min Sci, **48**, pp. 51-58, 2011.

[7] Lu, W.B. & Hustrulid, W., *An Improvement to the Equation for the Attenuation of the Peak Particle Velocity*, Engineering Blasting, **16**, pp. 49-53, 2002.

[8] Rao, Y.Z. & Wang, H., *Multiple Regression Linear Analysis on Attenuation of Blasting Vibration Velocity*, Metal Mine, **12,** pp. 46-51, 2013.

[9] Lu, T., Shi, Y-Q., Huang, C., Li, H-B., Xia, X., Zhou, Q-C. & Li, J-R. *Study on Attenuation Parameters of Blasting Vibration by Nonlinear Regression Analysis*, Rock and Soil Mechanics, **9**, pp. 1871-1878, 2007.

[10] Hu, J-H., Shang, J-L., Luo, X-W. & Zhou, K-P., *Monitoring of Single-hole Blasting Vibration and Detection of its Attenuation Law by Using Multiple Linear Regression*, Journal of Vibration and Shock, **16**, pp. 49-53, 2013.

[11] Demuth, H., Beal, M. & Hagan, M., *Neural Network Toolbox 5 User's Guide*, The Math Works, pp. 10-15, 1996.

[12] Maity, D. & Saha, A., *Damage Assessment in Structure from Changes in Static Parameters Using Neural Networks*, Sadhana, **29**, pp. 315-327, 2004.

[13] Dysart, P.S. & Pulli, J.J., *Regional Seismic Event Classification at the Noress Array: Seismological Measurements and the Use of Trained Neural Networks*, Bull. Seismol. Soc. Amer., **80**, pp. 1910-33, 1990.

[14] Rudajev, V. & Ciz, R., *Estimation of Mining Tremor Occurrence by Using Neural Networks*, Pure Appl. Geophys., **154**, pp. 57-72, 1999.

[15] Finnie, G.J., *Using Neural Networks to Discriminate between Genuine and Spurious Seismic Events in Mines*, Pure Appl. Geophys., **154**, pp. 41-56, 1999.
[16] Khandelwal, M. & Singh, T.N., *Prediction of Blast-induced Ground Vibration Using Artificial Neural Network*, Int. J. Rock. Mech. Min. Sci., **46**, pp. 1214-22, 2009.
[17] Monjezi, M. & Dehghani, H., *Evaluation of Effect of Blasting Pattern Parameters on Back Break Using Neural Networks*, Int. J. Rock. Mech. Min. Sci., **45**, pp. 1446-53, 2008.
[18] Khandelwal, M., Roy, M.P. & Singh, P.K., *Application of Artificial Neural Network in Mining Industry*, Indian Min. Eng. J., **43**, pp. 19-23, 2004.
[19] Maulenkamp, F. & Grima, M.A., *Application of Neural Networks for the Prediction of the Unconfined Compressive Strength (UCS) from Equotip Hardness*, Int. J. Rock. Mech. Min. Sci., **36**, pp. 29-39, 1999.
[20] Mohamed, M.T., *Artificial Neural Network for Prediction and Control of Blasting Vibrations in Assiut (Egypt) Limestone Quarry*, Int. J. Rock. Mech. Min. Sci., **46**, pp. 426-31, 2009.
[21] Tang, H. & Li, H.B., *Study of Blasting Vibration Formula of Reflecting Amplification Effect on Elevation*, J Rock and Soil Mechanics, **3**, pp. 820-824, 2011.
[22] Singh, T.N., Kanchan, R., Saigal, K. & Verma, A.K., *Prediction of P-wave Velocity and Anisotropic Properties of Rock Using Artificial Neural Networks Technique*, J Sci Indust Res, **63**, pp. 32-48, 2004.
[23] Rayleigh, J.W.S., *The Theory of Sound, Volume II*, Macmillan, London, United Kingdom, 1878.
[24] Khandelwal, M. & Singh, T.N., *Evaluation of Blast Induced Ground Vibration Predictors*, Soil Dynam Earthq Eng, **27**, pp. 116-125, 2007.
[25] Bellamine, F.H. & Elkamel, A., *Numerical Characterization of Distributed Dynamic Systems Using Tools of Intelligent Computing and Generalized Dimensional Analysis*, Appl Math Comp, **182**, pp. 1021-1039, 2006.
[26] Lu, H., Qi, C., Chen, Q., Gan, D., Xue, Z. & Hu, Y., *A New Procedure for Recycling Waste Tailings as Cemented Paste Backfill to Underground Stopes and Open Pits*, Journal of Cleaner Production, **188**, pp. 601-612, 2018.
[27] Bridgman, P., *Dimensional Analysis*, New Haven, London, United Kingdom, pp. 15-20, 1922.
[28] Ghosh, A. & Daemen, J.K., *A Simple New Blast Vibration Predictor*, In Proceedings of the 24th US Rock Mechanics Symposium, Texas A&M, **15**, pp. 151-161, 1983.
[29] Pal, P., *Putting Ground Vibration Predictors into Practice*, Colliery Guard, **241**, pp. 63-70, 1993.